Electronic flux densities in vibrating H_2^+ in terms of vibronic eigenstates

Jhon Fredy Pérez-Torres*
Institut für Chemie und Biochemie, Freie Universität Berlin, Takustraße 3, 14195 Berlin, Germany
(Received 22 February 2013; published 24 June 2013)

A theoretical study of the electronic and nuclear flux densities of a vibrating H_2^+ molecular ion is presented. The time-dependent wave function is represented in the basis of vibronic eigenstates which are numerically obtained from the complete nonrelativistic Hamiltonian without the clamped-nuclei approximation. A one-center expansion in terms of B-splines and Legendre polynomials is employed to solve the corresponding eigenvalue equation. The electronic and nuclear flux densities are then calculated from the total wave function through their quantum-mechanical definition. Analysis of the flux densities close to the turning points shows that the nuclear wave packet takes longer time (1.4 fs) to change its direction compared to the electronic one (1 fs).

DOI: 10.1103/PhysRevA.87.062512 PACS number(s): 31.15.ac, 31.15.ae, 31.15.xv

I. INTRODUCTION

Probability fluxes and flux densities are important in chemistry because they give detailed information about how reactants become products during a reaction. Probability flux refers to the amount of probability crossing a surface per unit time, whereas flux density is a vector quantity describing the flux of probability at a specific point at a given time. Calculation of electronic flux density (EFD; the $\mathbf{j}_e$ quantum observable) in molecules in a nonstationary state is not an easy task, simply because the customary practice of describing the state in the Born-Oppenheimer approximation (BOA) gives real electronic wave functions, for which EFD vanishes [1], although the probability flux does not. However, probability fluxes can be calculated from Gauss's theorem and the continuity equation making use of the electronic density in the BOA provided by standard quantum-chemistry calculations and nuclear quantum dynamics [2]. This approach of obtaining fluxes instead of flux densities was applied to a vibrating H_2^+ molecule in its electronic ground state [2–4] and successfully compared with accurate results obtained from non-Born-Oppenheimer calculations [2,5,6] yielding $\mathbf{j}_e \neq 0$. Probability flux calculations have been carried out for several systems, yielding unexpected results. For example, in the Cope rearrangement of semibullvalene, the nuclear probability flux revealed that breaking and formation of the carbon-carbon bond is synchronous, but the electronic probability flux associated with pericyclic orbitals shows an asynchronous behavior; that is, the electrons flow out of the breaking bond along the whole reaction (∼27.3 fs), and just at the end of the reaction they form the new bond [7,8]. Similar studies to that of semibullvalene have been carried out in pericyclic rearrangement of cyclooctatetraene [9]. More recently, electronic probability flux of vibrating ethane, ethene, and ethyne molecules revealed, in general, that more electrons participate in the concerted electron-nuclear vibrations in the case of ethane compared to that of ethene and ethyne [10]. Also, the effect of electron correlation on the electronic flux in vibrating H_2 molecules for different levels of quantum chemistry was addressed [11]. Thus, probability fluxes have become a valuable tool not only for studying synchronicity between nuclear and electronic motion in chemical reactions but also for calculating photoionization probabilities induced by electromagnetic fields [12]. However, how to calculate EFDs is still an open question, at least if one does not count the solution of the Schrödinger equation without the clamped-nuclei approximation (former step for the BOA), which is only available for H_2^+ [5,13–17] and H_2 [18] (only ground state) and, more recently, for H_2 [19] and H_2D^+ [20,21] (several states). At this point one should distinguish between electronic transition flux density and adiabatic EFD. The former is due to coherent superposition of two or more electronic states, i.e., electronic wave packets, and can be calculated within the BOA since the nuclear motion does not play a role in it [22–24]. The latter is due to the correlated motion between the nuclei and electrons and cannot be described in a straightforward form when the BOA is invoked. Approaches have been proposed to calculate EFDs induced by nuclear motion within the BOA framework. For example, Takatsuka and coworkers [25–27] have presented a semiclassical method which uses the Ehrenfest theory to synchronize the quantum electronic motion with a classical nuclear motion in order to calculate EFDs. Patchkovskii has analyzed the physical origin of the vanishing EFD when the BOA is invoked [28], finding that EFDs arise from the first-order nonadiabatic coupling to electronically excited states when a multistate Born-Huang ansatz [29] is employed. However, such flux densities involve excited electronic states and therefore refer to nonadiabatic EFD without the possibility of separating the transition flux density from the adiabatic one. Nevertheless, Diestler has developed a coupled-channel (CC) theory [30,31] to calculate the z component of the complete adiabatic EFD j_{ez} for a H_2^+ molecule oriented along the z axis and vibrating in its $^2\Sigma_g^+$ electronic ground state and, more recently, extended scaled coupled-channel (SCC) theory [32] to calculate the missing orthogonal component $j_{e\rho}$ while improving j_{ez} by using the continuity equation and taking advantage of cylindrical symmetry.

Scarce results on EFDs driven by nuclear motion, which are of increasing interest in developing techniques to access such flux densities, and, recently, the experimental deduction of nuclear flux densities from high-resolution pump-probe measurements in vibrating D_2^+ and Na_2 molecules [33] (which bodes well for future deduction of the EFDs) are the main

*jperez@zedat.fu-berlin.de

motivation of this investigation. Here a numerical representation of vibronic eigenstates without a clamped-nuclei approximation for H_2^+ molecule is presented. It is shown that such eigenstates are useful for calculating not only nuclear flux densities but also EFDs from their quantum-mechanical definition. This approach differs from the pioneering work [2] in that the EFDs can now be calculated in an arbitrary dense grid, especially on the internuclear axis and close to it. Bond formation and synchronicity between nuclear and electronic motion are also investigated.

II. DESCRIPTION OF THE METHOD

A. System

The full nonrelativistic Hamiltonian for the internal motion (Jacobi coordinates) of an oriented AB one-electron molecule is considered:

$$\mathcal{H} = -\frac{\hbar^2}{2\mu_n}\frac{d^2}{dR^2} + \frac{Z_a Z_b e^2}{4\pi\varepsilon_0 R} - \frac{\hbar^2}{2\mu_e}\nabla_r^2 - \frac{Z_a e^2}{4\pi\varepsilon_0 r_a} - \frac{Z_b e^2}{4\pi\varepsilon_0 r_b}, \tag{1}$$

with

$$\mu_e = \frac{m_e(m_a+m_b)}{m_a+m_b+m_e}, \quad \mu_n = \frac{m_a m_b}{m_a+m_b}, \tag{2}$$

$$R_a = \frac{m_b}{m_a+m_b}R, \quad R_b = \frac{m_a}{m_a+m_b}R, \tag{3}$$

$$r_a = |\mathbf{r}-\mathbf{R}_a|, \quad r_b = |\mathbf{r}-\mathbf{R}_b|, \tag{4}$$

and all the symbols having their usual meanings. Taking advantage of the cylindrical symmetry of the potential, the exact eigenstates of Hamiltonian (1) admit the following separation in spherical polar coordinates:

$$\psi_n^\Lambda(\mathbf{r},R) = \psi_n(r,\theta,R)\frac{e^{i\Lambda\phi}}{\sqrt{2\pi}}, \tag{5}$$

with $\hat{L}_z\psi_n^\Lambda(\mathbf{r},R) = \Lambda\psi_n^\Lambda(\mathbf{r},R)$ and $\hat{L}_z \equiv -i\hbar\partial/\partial\phi$, the z component of the electron angular momentum operator. For states with $^2\Sigma^+$ symmetry ($\Lambda = 0$), only two degrees of freedom remain for the electronic motion along the radial r and angular θ components (see Fig. 1), and therefore one needs to focus only on $\psi_n(r,\theta,R)$. By use of the multipole

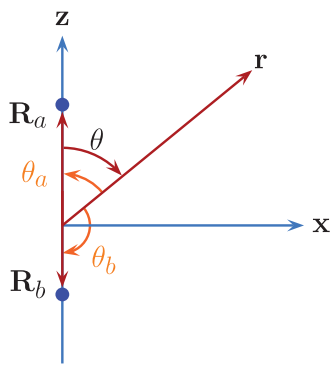

FIG. 1. (Color online) Polar coordinates (r,θ) for the electron. Molecule AB is oriented along the z axis.

expansion for the electron-nuclear attraction potential energy,

$$\frac{1}{|\mathbf{r}-\mathbf{R}_q|} = \sum_{\ell=0}^{\infty}\frac{r_{q<}^\ell}{r_{q>}^{\ell+1}}P_\ell(\cos\theta_q), \tag{6}$$

with $r_{q<} = \min(r,R_q)$ and $r_{q>} = \max(r,R_q)$, and the kinetic energy operator in spherical polar coordinates, Hamiltonian (1) is transformed into

$$\mathcal{H} = -\frac{\hbar^2}{2\mu_n}\frac{d^2}{dR^2} + \frac{Z_a Z_b e^2}{4\pi\varepsilon_0 R} - \frac{\hbar^2}{2\mu_e}\left[\frac{1}{r^2}\frac{\partial}{\partial r}\left(r^2\frac{\partial}{\partial r}\right)\right] + \frac{\hat{L}^2}{2\mu_e r^2} - \sum_{q=a,b}\frac{Z_q e^2}{4\pi\varepsilon_0}\sum_{\ell=0}^{\infty}\frac{r_{q<}^\ell}{r_{q>}^{\ell+1}}P_\ell(\cos\theta_q), \tag{7}$$

where $\hat{L}$ is the orbital angular momentum operator of the electron, given by

$$\hat{L}^2 = -\hbar^2\left[\frac{1}{\sin\theta}\frac{\partial}{\partial\theta}\left(\sin\theta\frac{\partial}{\partial\theta}\right) + \frac{1}{\sin^2\theta}\frac{\partial^2}{\partial\phi^2}\right], \tag{8}$$

P_ℓ are Legendre polynomials, $\cos\theta_a = \cos\theta$, and $\cos\theta_b = \cos(\pi-\theta) = -\cos\theta$ (see Fig. 1).

B. Energy eigensolutions

Eigenfunctions of the full Hamiltonian (7) are expanded in terms of the set of basis functions $\{\varphi_{ij\ell}\}$ according to

$$\psi_n(r,\theta,R) = \sum_{i=1}^{N_n}\sum_{j=1}^{N_e}\sum_{\ell=0}^{\ell_{\max}} b_{ij\ell}^n\varphi_{ij\ell}(r,\theta,R). \tag{9}$$

The basis functions consist of products of B-spline functions and Legendre polynomials describing the electronic motion with respect to the center of mass of the system (one-center expansion) and B-spline functions describing the relative motion of the protons

$$\varphi_{ij\ell}(r,\theta,R) = B_i^k(R)\frac{B_j^k(r)}{r}\chi_\ell(\theta), \tag{10}$$

$$\chi_\ell(\theta) = \sqrt{\frac{2\ell+1}{2}}P_\ell(\cos\theta), \tag{11}$$

$$\hat{L}^2\chi_\ell = \ell(\ell+1)\hbar^2\chi_\ell, \tag{12}$$

where $B_i^k(x)$ represents a B-spline function of order k defined within a box of length $x_{\max}$ [for simplicity, the index k is dropped for the φ function in Eq. (10) since it is previously set], N_n is the number of B splines describing the nuclear motion, N_e is the number of B splines describing the electronic motion, and $\ell_{\max}$ is the maximum value of the angular momentum. The one-center basis set method was used more than one decade ago to study photoionization of H_2^+ and H_2 [34,35] and more recently to study the effect of strong magnetic fields on H_2^+ [36]. B splines have been widely used in atomic and molecular physics [37]. By replacing the ansatz ψ_n in the time-independent Schrödinger equation the problem is then transformed into solving the secular equation:

$$(\mathtt{H}_{\lambda'\lambda} - \mathtt{S}_{\lambda'\lambda}E_n)\,b_\lambda^n = 0, \tag{13}$$

with

$$\mathtt{S}_{\lambda'\lambda} \equiv \mathtt{S}_{(ij\ell)'(ij\ell)} = S_{i'i}^n S_{j'j}^e\delta_{\ell'\ell}, \tag{14}$$

$$S^n_{i'i} = \int_0^{R_{\max}} B^k_{i'}(R) B^k_i(R) dR, \tag{15}$$

$$S^e_{j'j} = \int_0^{r_{\max}} B^k_{j'}(r) B^k_j(r) dr, \tag{16}$$

$$\mathtt{H}_{\lambda'\lambda} \equiv \mathtt{H}_{(ij\ell)'(ij\ell)}, \tag{17}$$

$$\mathtt{H}_{(ij\ell)'(ij\ell)} = \left[S^e_{j'j}\mathcal{O}^n_{i'i} + S^n_{i'i}\mathcal{O}^e_{j'j}\right]\delta_{\ell'\ell} - \sum_{q=a,b} \frac{Z_q e^2}{4\pi\varepsilon_0} \int_0^{R_{\max}} B^k_{i'}(R) V^q_{j'\ell' j\ell}(R) B^k_i(R) dR, \tag{18}$$

$$\mathcal{O}^n_{i'i} = \int_0^{R_{\max}} B^k_{i'}(R) \left[\frac{Z_a Z_b e^2}{4\pi\varepsilon_0 R} - \frac{\hbar^2}{2\mu_n}\frac{d^2}{dR^2}\right] B^k_i(R) dR, \tag{19}$$

$$\mathcal{O}^e_{j'j} = \int_0^{r_{\max}} B^k_{j'}(r) \left[\frac{\ell(\ell+1)\hbar^2}{2\mu_e r^2} - \frac{\hbar^2}{2\mu_e}\frac{d^2}{dr^2}\right] B^k_j(r) dr, \tag{20}$$

$$V^q_{j'\ell' j\ell}(R) = \sqrt{\frac{2\ell'+1}{2}}\sqrt{\frac{2\ell+1}{2}} \sum_{\ell''=0}^{2\ell_{\max}} \left\{\left[\int_0^{\pi} P_{\ell'}(\cos\theta) \times P_{\ell''}(\cos\theta_q) P_\ell(\cos\theta)\sin\theta d\theta\right] \times \left[\frac{\int_0^{R_q} B^k_{j'}(r) r^{\ell''} B^k_j(r) dr}{R_q^{\ell''+1}} + R_q^{\ell''} \int_{R_q}^{r_{\max}} \frac{B^k_{j'}(r) B^k_j(r)}{r^{\ell''+1}} dr\right]\right\}, \tag{21}$$

and $R_{\max}$ and $r_{\max}$ being the lengths of the boxes for electronic and nuclear motion, respectively. Because of the properties of the B splines [$B^k_i(x)B^k_j(x) = 0$ for $|i-j| \leqslant k$] [38], $\mathtt{S}_{\lambda'\lambda}$ and $\mathtt{H}_{\lambda'\lambda}$ are sparse matrices, thus facilitating the solution of the eigenvalue problem using PETSC [39] and SLEPC [40] routines that are optimized for parallel processing.

Note that functions ψ_n correspond to vibronic states of the molecule without the clamped-nuclei Hamiltonian approximation. Thus correlation between the nuclear and electronic motion is fully accounted for.

C. Coupled electron-nuclear dynamics

In order to study the dynamics of a vibrating $H_2{}^+$ molecule (in a nonstationary state), the initial time-dependent wave function is taken to be

$$\Psi(r,\theta,R,t=0) = \psi_0(r,\theta,R-\bar{R}), \tag{22}$$

where $\psi_0(r,\theta,R-\bar{R})$ is the vibronic ground-state energy eigenfunction displaced by $\bar{R}$ in the same way as in [2,31]. The created wave packet can then be expanded in terms of the vibronic eigenfunctions as

$$\Psi(r,\theta,R,t) = \sum_n c_n \psi_n(r,\theta,R) e^{-iE_n t/\hbar} \tag{23}$$

with

$$c_n = \langle\psi_n|\Psi(t=0)\rangle. \tag{24}$$

The probability density distribution for the electron can be calculated as

$$\rho_e(r,\theta,t) = \int_0^{R_{\max}} \Psi^*(r,\theta,R,t)\Psi(r,\theta,R,t) dR = \sum_{mn} c_m c_n \cos(\omega_{mn} t) \times \int_0^{R_{\max}} \psi_m(r,\theta,R)\psi_n(r,\theta,R) dR, \tag{25}$$

with $\omega_{mn} = (E_m - E_n)/\hbar$ being the Bohr frequency, whereas the EFD associated to the wave packet Ψ at time t is given by

$$\begin{aligned}\mathbf{j}_e(r,\theta,t) &= \frac{\hbar}{\mu_e}\mathrm{Im}\left[\int_0^{R_{\max}} \Psi^*(r,\theta,R,t)\nabla_{\mathbf{r}}\Psi(r,\theta,R,t) dR\right] \\ &= \frac{\hbar}{\mu_e}\sum_{mn} c_m c_n \sin(\omega_{mn} t) \times \left\{\left[\int_0^{R_{\max}} \psi_m(r,\theta,R)\frac{\partial}{\partial r}\psi_n(r,\theta,R) dR\right]\mathbf{e}_r + \left[\int_0^{R_{\max}} \psi_m(r,\theta,R)\frac{\partial}{r\partial\theta}\psi_n(r,\theta,R) dR\right]\mathbf{e}_\theta\right\} \\ &\equiv j_{er}(r,\theta,t)\mathbf{e}_r + j_{e\theta}(r,\theta,t)\mathbf{e}_\theta,\end{aligned} \tag{26}$$

where Im stands for the imaginary part. The vector field $\mathbf{j}_e = j_{er}\mathbf{e}_r + j_{e\theta}\mathbf{e}_\theta$ can be transformed to Cartesian coordinates according to

$$\begin{pmatrix} j_{ex} \\ j_{ez}\end{pmatrix} = \begin{pmatrix} \sin\theta & \cos\theta \\ \cos\theta & -\sin\theta\end{pmatrix}\begin{pmatrix} j_{er} \\ j_{e\theta}\end{pmatrix}. \tag{27}$$

Similarly, for the nuclear motion, the probability density distribution and the flux density read, respectively,

$$\rho_n(R,t) = \sum_{mn} c_m c_n \cos(\omega_{mn} t)\left[\int_0^{r_{\max}}\int_0^{\pi} r^2 \sin\theta \, \psi_m(r,\theta,R)\psi_n(r,\theta,R) dr d\theta\right], \tag{28}$$

$$j_n(R,t) = \frac{\hbar}{\mu_n}\sum_{mn} c_m c_n \sin(\omega_{mn} t)\left[\int_0^{r_{\max}}\int_0^{\pi} r^2 \sin\theta \, \psi_m(r,\theta,R)\frac{d}{dR}\psi_n(r,\theta,R) dr d\theta\right]. \tag{29}$$

It should be remarked that ρ_e, ρ_n, and j_n can be obtained from wave functions within the BOA framework, but not $\mathbf{j}_e$. Moreover Eqs. (26) and (29) deserve some comments. First, the diagonal terms $m = n$ vanish; i.e., there is a vanishing quantum-mechanical flux density when a pure vibronic state is prepared ($c_n = \delta_{mn}$) even if the clamped-nuclei approximation is not invoked, and this observation is valid as well for many-body systems in the absence of external fields [1]. Second, when only two states are taken into account in the summation, the resulting flux corresponds to the "transition current density" defined by Nafie [22]. Thus the flux densities calculated here can be considered the multistate transition flux density among vibronic eigenstates. Finally, it should be

pointed out that by construction Ψ satisfies the continuity equation ($\nabla \cdot \mathbf{j} + \partial_t \rho = 0$), which serves in the analysis of the SCC theory [32].

III. RESULTS

All results reported here correspond to a basis set of $N_e = 35$ and $N_n = 60$ B-spline functions of order $k = 8$ with a linear knot sequence and with a box length of $r_{\max} = R_{\max} = 10a_0$ for the electronic and nuclear motion, respectively. For the angular part of the electron, Legendre polynomials up to $\ell_{\max} = 16$ have been included. Despite the slow convergence problem of the one-center method with $\ell_{\max}$ for large internuclear distance, calculations of molecular orbitals of $H_2{}^+$ with $\ell_{\max} = 8$ yield good results in the range $R = 0$–$5a_0$ [41]. A proton-electron mass ratio of $m_p/m_e = 1836.15267245$ has been used [42]. Calculated energies of the $^2\Sigma_g^+$ states are shown in Table I and are compared with converged results from Ref. [15]. In general, energies reported here are not very accurate. However, the goal of the present work is to calculate flux densities and not accurate energy levels with metrological applications (the ratio m_p/m_e of the proton mass to the electron mass can be deduced from a high-precision measurement of a transition between two different $H_2{}^+$ rovibrational levels). In order to set the dynamics of a vibrating $H_2{}^+$ molecule, the bond is initially stretched by the distance $\bar{R}$ from its equilibrium length; i.e., the ground-state wave function is shifted by $\bar{R} = 2a_0$ in the same way as in [2,31], thus creating a vibronic wave packet at $t = 0$. Then the time-dependent wave function is represented by Eq. (23). The summation is restricted to those states with energies below the first dissociation threshold ($-0.499727840 E_h$) in order to avoid dissociation and electronic excitation in the context of the BOA. The coefficients c_n of the wave packet are also listed in Table I. Notice that the energies of the states from $n = 4$ to $n = 9$ (the ones contributing mainly to the wave packet) are in good agreement to three digits.

TABLE I. Energies E_n in Hartrees of the bound states obtained with the basis set: $N_e = 35$, $\ell_{\max} = 16$, and $N_n = 60$ (this work). Coefficients c_n corresponding to the vibronic wave packet [Eq. (23)] are also shown. * Bound states not converged, i.e., their energies lie above the dissociation threshold (-0.499727840 E_h).

n	E_n (this work)	E_n (Ref. [15])	c_n (this work)
0	−0.596 751 915 816	−0.597 139 063 079	0.000 140
1	−0.586 793 129 762	−0.587 155 679 096	0.001 437
2	−0.577 473 370 487	−0.577 751 904 415	−0.008 927
3	−0.568 634 422 997	−0.568 908 498 731	0.039 921
4	−0.560 375 035 881	−0.560 609 220 850	−0.128 628
5	−0.552 563 334 751	−0.552 840 749 897	0.305 858
6	−0.545 265 214 380	−0.545 592 650 994	0.531 927
7	−0.538 475 685 415	−0.538 857 386 968	−0.626 807
8	−0.532 114 235 481	−0.532 630 379 356	−0.442 295
9	−0.526 252 860 512	−0.526 910 124 016	0.101 574
10	−0.520 836 155 017	−0.521 698 369 014	0.073 725
11	−0.515 857 453 582	−0.517 000 365 279	−0.016 440
12	−0.511 353 243 839	−0.512 825 203 146	0.025 307
13	−0.507 243 531 683	−0.509 186 248 369	−0.008 684
14	−0.503 566 834 118	−0.506 101 680 969	−0.002 267
15	−0.500 257 363 323	−0.503 595 084 999	0.005 225
16	*	−0.501 695 773 387	*
17	*	−0.500 437 040 460	*
18	*	−0.499 837 432 030	*
19	*	−0.499 731 230 649	*

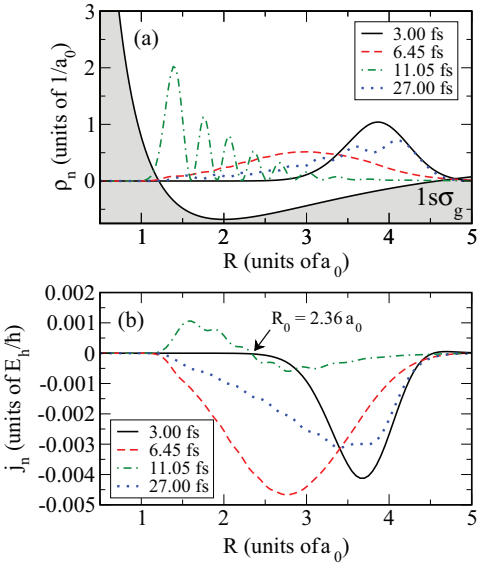

FIG. 2. (Color online) Nuclear densities at characteristic times 3.00, 6.45, 11.05, and 27.00 fs. (a) Nuclear probability densities superposed on a plot of the ground-state Born-Oppenheimer potential energy curve; (b) nuclear flux densities.

Figure 2 display plots of the nuclear probability density [Fig. 2(a)] and nuclear flux density [Fig. 2(b)]. Results at 3.00, 6.45, and 11.05 fs are in good agreement with those based on the BOA reported in [31]. Results for 27.00 fs are also shown. From 3.00 to 6.45 fs the nuclear wave packet is dispersed, covering the region from the inner to the outer turning point, and the nuclear flux density is negative for all values of R, corresponding to bond compression. At 11.05 fs the nuclear probability density displays the characteristic pattern of quantum interference caused by partial waves traveling in opposite directions. This is corroborated by the nuclear flux density, which changes sign at $R_0 = 2.36a_0$ at 11.05 fs, corresponding to a transition from bond shortening to bond lengthening. Thus a node in the nuclear flux density (hereby named the wave front) can be identified around

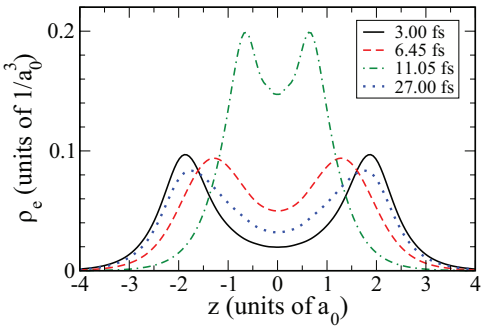

FIG. 3. (Color online) Electronic probability densities along the internuclear axis ($x = 0, y = 0$) for the characteristic times 3.00, 6.45, 11.05, and 27.00 fs.

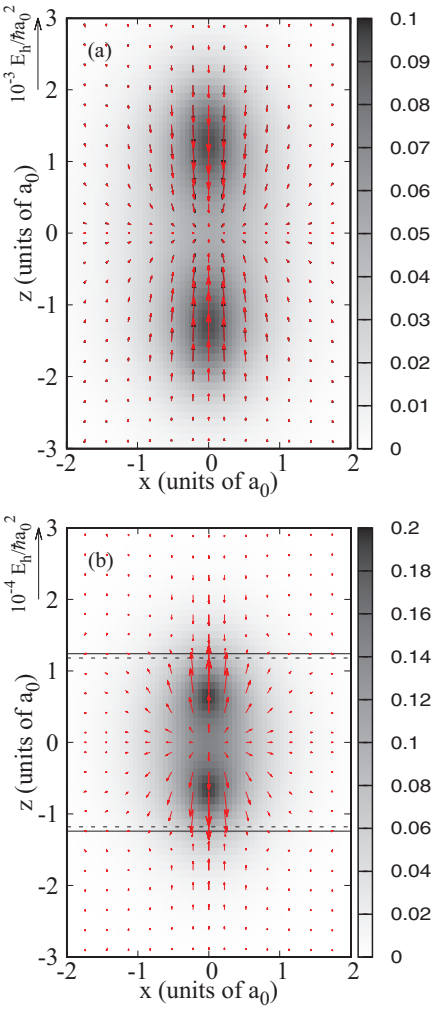

FIG. 4. (Color online) Electronic flux densities: (a) At $t = 6.45$ fs for the present results [red (gray) arrows] and results from [2] (black arrows). (b) At $t = 11.05$ fs for the present results [red (gray) arrows]; the two solid horizontal lines indicate the electronic wave front located at $z = \pm 1.24a_0$, and the two dashed horizontal lines indicate the nuclear wave front located at $z = \pm 1.18a_0$ [$R_0/2$; see Fig. 2 (b)]. Electronic probability densities are shown as a contour plot.

$z = \pm R_0/2 = \pm 1.18a_0$ [see Fig. 2(b)]. At 27.00 fs the nuclear flux density reveals complete bond compression again (flux density negative for all R values).

Figure 3 displays the electronic probability density along the internuclear axis for times 3.00, 6.45, 11.05, and 27.00 fs. Notice that the electronic wave packet does not show the interference pattern during the reflection as the nuclear wave packet does. This is because the electronic wave packet is more delocalized than the nuclear wave packet, and hence the electronic interference pattern is washed out by the nuclear motion. At 27.00 fs there is a significant enhancement of the electronic probability density along the internuclear axis. This bond formation is due to the dispersion of the nuclear wave packet (see the nuclear probability density at 27.00 fs in Fig. 2); thus the dispersion of the nuclear wave function is accompanied by a σ-bond formation.

Figure 4 displays the EFD (vector plot) in the xz plane at two different times, 6.45 and 11.05 fs. The electronic

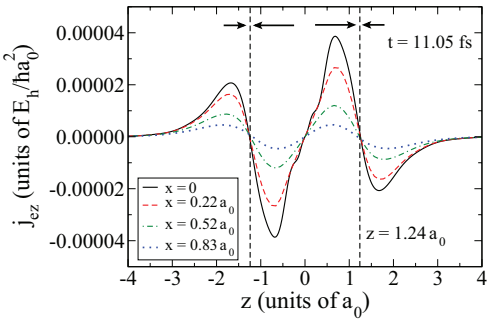

FIG. 5. (Color online) The z component of the electronic flux density j_{ez} as a function of z for $x = 0$, $x = 0.22a_0$, $x = 0.52a_0$, and $x = 0.83a_0$ at $t = 11.05$ fs. The arrows represent the direction of the flux, and the vertical dashed lines represent the wave front.

probability densities are also shown as a contour plot. In general, $\mathbf{j}_e$ consists of a dominant j_{ez} component (along the z axis where the nuclear motion takes place) and a weaker j_{ex} component. At 6.45 fs the EFD is in good agreement with that of [2] except for small deviations when $x \to 0$. Nevertheless, the flux density calculated here shows the correct behavior ($j_{ex} \to 0$ when $x \to 0$). At 11.05 fs a nodal line in the EFD can be seen (solid lines), which is associated with the wave front that reflects the nuclear motion (dashed lines). This can be best appreciated from Fig. 5, which displays the z component of the EFD as a function of z for several values of x at $t = 11.05$ fs. Notice that the position of the electronic wave front is essentially independent of the x coordinate (i.e., it resembles a plane-wave front). Also notice that the wave front for the electronic wave packet at 11.05 fs is located (at $z = \pm 1.24a_0$) beyond the wave front of the nuclear wave packet (at $z = \pm 1.18a_0$); see Fig. 4(b). This displacement and the fact that the electron wave packet changes direction before the nuclear wave packet reinforce the results reported in [2–4] obtained from the probability fluxes. The electron does not

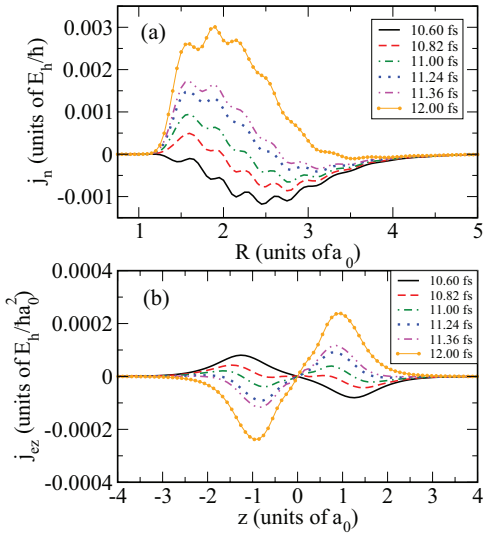

FIG. 6. (Color online) Flux densities at different times: (a) nuclear flux density as a function of R; (b) z component of the electronic flux density j_{ez} as a function of z for $x = 0$.

necessarily respond instantly to the nuclear motion, as one may predict from the BOA.

Figure 6 shows the nuclear flux density and EFD along the internuclear axis for different times as the electronic and nuclear wave packets change direction completely. Observe that the reflection of the electronic wave packet takes basically less than 1 fs (from approximately $t = 10.60$ to $t = 11.36$ fs), while the total reflection of the nuclear wave packet takes at least more than 1.4 fs (from approximately $t = 10.60$ to $t = 12.00$ fs). This characteristic delay in the attosecond time scale is in good agreement with the delay between the electronic and nuclear fluxes (with opposite directions) reported in [2]. This is again a consequence of the faster dispersion of the nuclear wave packet compared to the electronic one.

IV. SUMMARY

A method to calculate electronic and nuclear flux densities from their quantum-mechanical definition in an oriented vibrating $H_2{}^+$ molecule is presented. The results agree well with previous accurate results [2]. The time-dependent wave function was expanded in the basis of vibronic energy eigenstates obtained without the clamped-nuclei approximation, thus accounting for the correlated electron-nuclei dynamics. The expansion was restricted to vibronic eigenstates whose energies lie below the first dissociation threshold. Therefore the resulting EFDs can be ascribed entirely to adiabatic electronic flux densities in the context of the framework of the BOA (i.e., an EFD induced exclusively by the nuclear motion in the $1s\,\sigma_g$ potential energy curve). Analysis of flux densities reveals asynchronicity between electronic and nuclear motion close to the turning points happening in the attosecond time scale, an effect already discovered elsewhere [2]. It is hoped that the method developed here serves as a useful tool for judging the quality of different approximate approaches to computing the EFD since it not only provides the EFD in an arbitrary grid but also accounts for the continuity equation at any point. Calculations of EFDs for vibration and dissociation in asymmetric systems such as HD^+, HT^+, and DT^+ are being pursued.

ACKNOWLEDGMENTS

The author is very thankful to Professor J. Manz (Freie Universität Berlin, Germany) and Professor D. Diestler (University of Nebraska–Lincoln, United States) for very helpful and stimulating discussions. Freie Universität Berlin (FUB) and Scientific Computing Services Unit of the Zentraleinrichtung für Datenverarbeitung (ZEDAT) at FUB are gratefully acknowledged for financial support and allocation of computer time. This work profited from financial support of project Ma 515/25-1 of the Deutsche Forschungsgemeinschaft.

[1] E. Schrödinger, Ann. Phys. (Leipzig) **81**, 109 (1926).
[2] I. Barth, H.-C. Hege, H. Ikeda, A. Kenfack, M. Koppitz, J. Manz, F. Marquardt, and G. K. Paramonov, Chem. Phys. Lett. **481**, 118 (2009).
[3] A. Kenfack, F. Marquardt, G. K. Paramonov, I. Barth, C. Lasser, and B. Paulus, Phys. Rev. A **81**, 052502 (2010).
[4] A. Kenfack, I. Barth, F. Marquardt, and B. Paulus, Phys. Rev. A **82**, 062502 (2010).
[5] G. K. Paramonov, Chem. Phys. Lett. **411**, 350 (2005).
[6] G. K. Paramonov, Chem. Phys. **338**, 329 (2007).
[7] D. Andrae, I. Barth, T. Bredtmann, H.-C. Hege, J. Manz, F. Marquardt, and B. Paulus, J. Phys. Chem. B **115**, 5476 (2011).
[8] T. Bredtmann and J. Manz, Angew. Chem., Int. Ed. **50**, 12652 (2011).
[9] H.-C. Hege, J. Manz, F. Marquardt, B. Paulus, and A. Schild, Chem. Phys. **376**, 46 (2010).
[10] T. Bredtmann, E. Hupf, and B. Paulus, Phys. Chem. Chem. Phys. **14**, 15494 (2012).
[11] A. Kenfack, S. Banerjee, and B. Paulus, Phys. Rev. A **85**, 032501 (2012).
[12] P. von den Hoff, I. Znakovskaya, S. Zherebtsov, M. F. Kling, and R. de Vivie-Riedle, Appl. Phys. B **98**, 659 (2010).
[13] H. Kono, Y. Sato, M. Kanno, K. Nakai, and T. Kato, Bull. Chem. Soc. Jpn. **79**, 196 (2006).
[14] S. Chelkowski, T. Zuo, O. Atabek, and A. D. Bandrauk, Phys. Rev. A **52**, 2977 (1995).
[15] J. P. Karr and L. Hilico, J. Phys. B **39**, 2095 (2006).
[16] T. Niederhausen, U. Thumm, and F. Martín, J. Phys. B **45**, 105602 (2012).
[17] A. Ishikawa, H. Nakashima, and H. Nakatsuji, Chem. Phys. **401**, 62 (2012).
[18] B. Chen and J. B. Anderson, J. Chem. Phys. **102**, 2802 (1995).
[19] S. Bubin, F. Leonarski, M. Stanke, and L. Adamowicz, Chem. Phys. Lett. **477**, 12 (2009).
[20] E. Mátyus, J. Hutter, U. Müller-Herold, and M. Reiher, J. Chem. Phys. **135**, 204302 (2011).
[21] E. Mátyus and M. Reiher, J. Chem. Phys. **137**, 024104 (2012).
[22] L. A. Nafie, J. Phys. Chem. A **101**, 7826 (1997).
[23] T. B. Freedman, X. Gao, M.-L. Shih, and L. A. Nafie, J. Phys. Chem. A **102**, 3352 (1998).
[24] I. Barth, J. Manz, Y. Shigeta, and K. Yagi, J. Am. Chem. Soc. **128**, 7043 (2006).
[25] M. Okuyama and K. Takatsuka, Chem. Phys. Lett. **476**, 109 (2009).
[26] K. Nagashima and K. Takatsuka, J. Phys. Chem. A **113**, 15240 (2009).
[27] K. Takatsuka and T. Yonehara, Phys. Chem. Chem. Phys. **13**, 4987 (2011).
[28] S. Patchkovskii, J. Chem. Phys. **137**, 084109 (2012).
[29] M. Born and K. Huang, *Dynamical Theory of Crystal Lattices* (Oxford University Press, Oxford, 1954).
[30] D. J. Diestler, J. Phys. Chem. A **116**, 2728 (2012).
[31] D. J. Diestler, A. Kenfack, J. Manz, and B. Paulus, J. Phys. Chem. A **116**, 2736 (2012).
[32] D. J. Diestler, A. Kenfack, J. Manz, B. Paulus, J. F. Pérez-Torres, and V. Pohl, J. Phys. Chem. A (2013), doi: 10.1021/jp4002302.

[33] J. Manz, J. F. Pérez-Torres, and Y. Yang (unpublished).
[34] M. Brosolo, P. Decleva, and A. Lisini, J. Phys. B **25**, 3345 (1992).
[35] F. Martín, J. Phys. B **32**, R197 (1999).
[36] Y. Zhang, Q. Liu, and T. Shi, J. Phys. B **45**, 085101 (2012).
[37] H. Bachau, E. Cormier, P. Decleva, J. E. Hansen, and F. Martín, Rev. Prog. Phys. **64**, 1601 (2001), and references therein.
[38] C. de Boor, *A Practical Guide to Splines* (Springer, New York, 1978).
[39] S. Balay, K. Buschelman, W. D. Gropp, D. Kaushik, M. G. Knepley, L. C. McInnes, B. F. Smith, and H. Zhang, PETSC, http://www.mcs.anl.gov/petsc.
[40] V. Hernandez, J. E. Roman, and V. Vidal, ACM Trans. Math. Software **31**, 351 (2005), http://www.grycap.upv.es/slepc/.
[41] I. Sánchez and F. Martín, Phys. Rev. A **57**, 1006 (1998).
[42] CODATA internationally recommended values of the fundamental physical constants, http://physics.nist.gov/cuu/Constants/.